

Effect of gold doping on relativistic electron beam transport in high-density plasma

Zi-Yan Zhang(张子彦) and Wei-Min Wang(王伟民)

Citation: Chin. Phys. B, 2025, 34 (**7**): 075201. DOI: 10.1088/1674-1056/add4df
http://cpb.iphy.ac.cn; http://iopscience.iop.org/cpb

What follows is a list of articles you may be interested in

Suppression of the Kelvin-Helmholtz instability by coating in the double-cone ignition scheme

Yuan-Kai Xie(谢元凯), Cheng-Long Zhang(张成龙), Yi-Zhen Cheng(程翊真), and Ying-Jun Li(李英骏)
Chin. Phys. B, 2024, 33 (**12**): 125203. DOI: 10.1088/1674-1056/ad8551

A model for fast electron-driven high-density plasma in the double-cone ignition scheme

Zhong-Yi Chen(陈忠义), Kai-Ge Zhao(赵凯歌), and Ying-Jun Li(李英骏)
Chin. Phys. B, 2024, 33 (**11**): 115202. DOI: 10.1088/1674-1056/ad71b8

Development of a monochromatic crystal backlight imager for the recent double-cone ignition experiments

Chenglong Zhang(张成龙), Yihang Zhang(张翌航), Xiaohui Yuan(远晓辉), Zhe Zhang(张喆), Miaohua Xu(徐妙华), Yu Dai(戴羽), Yufeng Dong(董玉峰), Haochen Gu(谷昊琛), Zhengdong Liu(刘正东), Xu Zhao(赵旭), Yutong Li(李玉同), Yingjun Li(李英骏), Jianqiang Zhu(朱健强), and Jie Zhang(张杰)
Chin. Phys. B, 2024, 33 (**2**): 025201. DOI: 10.1088/1674-1056/ad1091

Effect of tearing modes on the confinement of runaway electrons in Experimental Advanced Superconducting Tokamak

Rui-Jie Zhou(周瑞杰)
Chin. Phys. B, 2023, 32 (**7**): 075204. DOI: 10.1088/1674-1056/acc3f8

Measurement of molybdenum ion density for L-mode and H-mode plasma discharges in the EAST tokamak

Yongcai Shen(沈永才), Hongming Zhang(张洪明), Bo Lyu(吕波), Yingying Li(李颖颖), Jia Fu(符佳), Fudi Wang(王福地), Qing Zang(臧庆), Baonian Wan(万宝年), Pan Pan(潘盼), Minyou Ye(叶民友)
Chin. Phys. B, 2020, 29 (**6**): 065206. DOI: 10.1088/1674-1056/ab8456

RAPID COMMUNICATION

Effect of gold doping on relativistic electron beam transport in high-density plasma

Zi-Yan Zhang(张子彦)[1,2] and Wei-Min Wang(王伟民)[1,2,3,†]

[1] *School of Physics and Beijing Key Laboratory of Opto-electronic Functional Materials and Micro-nano Devices, Renmin University of China, Beijing* 100872, *China*

[2] *Key Laboratory of Quantum State Construction and Manipulation (Ministry of Education), Renmin University of China, Beijing* 100872, *China*

[3] *Key Laboratory for Laser Plasmas & School of Physics and Astronomy, Shanghai Jiao Tong University, Shanghai* 200240, *China*

(Received 25 February 2025; revised manuscript received 22 April 2025; accepted manuscript online 7 May 2025)

We investigate the influence of gold doping on the transport range of a relativistic electron beam in high-density deuterium–tritium (DT) fuel, which could be encountered in the double-cone ignition laser fusion. We develop the stopping power model to include gold doping and then analyze the influence of Coulomb collision and bremsstrahlung on the electron transport range with different gold doping ratios, consistent with the Geant4 simulations. When the gold doping ratio increases from 0.5% to 30%, the transport range of a 10 MeV electron beam is decreased by 9.6% and 18.5% via the bremsstrahlung. For the 1 MeV beam, the decrease of the range becomes 0.7% and 1.0%. We also investigate the transverse broadening of the electron beam and radiated photon energy reabsorption in a spherical target. When the gold doping ratio is 2% and the beam energy is increased from 1 MeV to 5 MeV, the bremsstrahlung photons cover 2.6% to 10.3% of the total beam energy. Meanwhile, the reabsorbed photon energy is reduced from 31.6% to 8.9%.

Keywords: double-cone ignition (DCI) scheme, stopping power, Geant4, bremsstrahlung

PACS: 52.57.Kk, 52.20.Hv, 52.65.Pp

DOI: 10.1088/1674-1056/add4df **CSTR:** 32038.14.CPB.add4df

1. Introduction

Laser driven inertial confinement fusion (ICF),[1–7] as one of the main controlled nuclear fusion approaches, has been widely studied[8–14] and made major progress since it was proposed. Via the mainstream indirect-driving central ignition scheme, fusion ignition has been experimentally achieved a few times at the National Ignition Facility (NIF) in the USA[15–17] since December 2022. Aiming for higher energy gains with smaller energy laser drivers, scientists are still exploring other ICF schemes, e.g., the fast ignition (FI) scheme[18–24] as a direct-driving non-central ignition one, which separates the heating from the target compression. In 2020, Zhang *et al.* proposed the double-cone ignition (DCI) scheme[25] to achieve quasi-isentropic compression, which in principle is favorable for the heating by the ps laser driven relativistic electron beams, and to enhance the laser target coupling via a magnetically guided ignition approach.[26] The DCI scheme could significantly reduce the laser energy demand and improve the stability of the compression. Recently, the feasibility of the DCI scheme has been demonstrated.[27–34]

In the DCI scheme,[25] the fuel is compressed in two head-on guide gold cones and gold doping in the deuterium–tritium (DT) fuel is hard to avoid. In the cone-inserted FI scheme,[35] a gold cone is applied and there is also some gold doping in the DT. The relativistic electron beams generated by the ps laser pulse could significantly lose energy through bremsstrahlung when they are transported in the DT fuel doped with gold with a high-atomic number. Here, we investigate the effect of gold doping on the transport range or deposition position of the relativistic electron beam in the context of the DCI scheme or fast ignition with a gold cone inserted.[35] We calculate the electron range using the stopping power model and Monte Carlo (MC) simulations with the Geant4,[36] which is an open code to accurately simulate the electron beam transport. The stopping power model assumes a continuous loss of electron energy based on the continuous slowing down approximation. Deutsch *et al.*[37] developed the model with Coulomb collision and the collective effect of plasma included. Based on the improved model by Li and Petrasso,[38–40] Solodov and Betti[41] further developed the collision scattering cross section to more accurately calculate the electron transport range. In 2009, Atzenti *et al.*[42] incorporated the plasma screen effect to the model.

Here, we develop the stopping power model to include the contribution of gold doping, i.e., considering the impact of the gold doping on the mean scattering angle and bremsstrahlung energy loss. The deposition position of electron beams is analyzed by the model and verified by Geant4 simulations to ensure reliability. We calculate the electron longitudinal range

[†]Corresponding author. E-mail: weiminwang1@ruc.edu.cn

© 2025 Chinese Physical Society and IOP Publishing Ltd. All rights, including for text and data mining, AI training, and similar technologies, are reserved.

with different gold doping ratios to quantify the respective contributions of Coulomb collisions and the bremsstrahlung to the electron energy deposition. In addition, we investigate the transverse broadening of the electron beam and radiated photon energy reabsorption in a real spherical target with a typical areal density of 1 g/cm^2. It is shown that the electron energy deposition and the radiation energy loss strongly depend on the initial electron energy when there is appreciable gold doping.

The paper is organized as follows. In Section 2, the stopping power model with gold doping effects is developed to investigate the energy deposition of a relativistic electron beam in DT fuel, and the stopping power calculation results are benchmarked by Geant4. Then, we employ the model to calculate the contributions of Coulomb collision and bremsstrahlung to the electron transport ranges in Section 3. In Section 4, utilizing the Geant4 simulation, we present the transverse broadening of the electron beam and the reabsorption of energy from radiated photons within a realistic spherical target. Finally, a brief summary is given in Section 5.

2. Stopping power model with electron–gold collision and bremsstrahlung

In the DCI and cone-inserted FI, it is hard to avoid gold doping in the DT plasma, and therefore, the impact of gold doping on relativistic electron beam transport in the fuel should be considered. We develop the stopping power model to investigate the electron transport in gold doped DT fuel with the bremsstrahlung energy loss and electron–gold collision included, based on the conventional stopping power model in pure DT fuel. Without the gold doping, the electron range shows little difference between the stopping power model and Geant4 simulation with the relativistic electron beam of 0.3 MeV to 10 MeV in the fuel with the density of 50 g/cm^3 to 300 g/cm^3, as illustrated in Appendix A. Our investigation shows that when the gold doping is considered, the scattering angle of Coulomb collisions between electrons and ions is enhanced and the electron energy loss is increased due to the bremsstrahlung.

We utilize the electron energy loss rate $\mathrm{d}E/\mathrm{d}s$ and the first-order spatial moments of the electron distribution function $\langle P_1(\cos\theta)\rangle = \langle\cos\theta\rangle$, which represent the energy loss of the electron with its trajectory and the mean scattering angle via collisions,[43] respectively. Then, the energy loss of the electron along the transport path is given by

$$\frac{\mathrm{d}E}{\mathrm{d}x} = \langle\cos\theta\rangle^{-1}\frac{\mathrm{d}E}{\mathrm{d}s}, \tag{1}$$

and the electron transport range is given by[41]

$$\langle x\rangle = \int_{E_0}^{E_1}\langle\cos\theta\rangle\left(\frac{\mathrm{d}E}{\mathrm{d}s}\right)^{-1}\mathrm{d}E, \tag{2}$$

where the mean scattering angle

$$\langle\cos\theta\rangle = \exp\left[-\int_0^s \kappa_1(s')\,\mathrm{d}s'\right]$$

is related to the transport scattering cross sections $\kappa_1(s) = \kappa_1^{\mathrm{e}}(s) + \kappa_1^{\mathrm{i}}(s)$ and e and i represent electron–electron and electron–ion collisions, respectively. The deflection of electron trajectories is mainly caused by Coulomb collisions with ions in dense plasma. When gold is doped into DT fuel, the electron–ion collision transport scattering cross section is $\kappa_1^{\mathrm{i}} = \kappa_1^{\mathrm{DT}} + \kappa_1^{\mathrm{Au}}$. Due to $\kappa_1^{\mathrm{i}} \propto n_{\mathrm{i}}Z^2$, the high Z gold causes the collision frequency to be dramatically enhanced and the mean free path of electron collision to be significantly reduced.

In addition to the electron–gold collision effect, bremsstrahlung can also affect the relativistic electron beam energy deposition in gold doped fuel. The Bethe–Bloch theory states that the bremsstrahlung losses can be described in terms of average energy loss per unit path length $\mathrm{d}E/\mathrm{d}x$. Seltzer *et al.*[44,45] combined the theoretical investigation of calculating bremsstrahlung cross sections in the field of the electron and atomic nucleus to give the integrated radiative energy-loss cross section $\Phi_{\mathrm{rad}}^{\mathrm{total}}$. The reduction of electron transport range by bremsstrahlung can be clearly seen in the radiative energy loss rate of electrons. The electron linear energy loss rate is

$$\begin{aligned}-\frac{\mathrm{d}E}{\mathrm{d}s} = {}& \frac{2\pi r_0^2 mc^2 n_{\mathrm{e}}}{\beta^2}\left\{\ln\left[\left(\frac{E}{\hbar\omega_{\mathrm{p}}}\right)^2\frac{(\gamma+1)}{2\gamma^2}\right]\right.\\ &\left.+1+\frac{1}{8}\left(\frac{\gamma-1}{\gamma}\right)^2-\left(\frac{2\gamma-1}{\gamma^2}\right)\ln 2\right\}\\ &+n_{\mathrm{i}}\left(\alpha r_0^2\right)\left(E+mc^2\right)Z^2\Phi_{\mathrm{rad}}^{\mathrm{total}},\end{aligned} \tag{3}$$

where $r_0 = e^2/(mc^2)$ is the classical electron radius, m is the electron mass, n_{e} and n_{i} are the electron and ion number densities, $\beta = v/c$ is the electron velocity normalized to the speed of light c, $\gamma = (1-\beta^2)^{-1/2}$, $E = mc^2(\gamma-1)$, $\omega_{\mathrm{p}} = \sqrt{4\pi n_{\mathrm{e}}e^2/m_{\mathrm{e}}}$, and α is the fine-structure constant. Here, the first term on the right-hand side represents the Coulomb collisions and plasma wave excitation. The second term represents bremsstrahlung radiation contributions. We then substitute Eq. (3) into Eq. (2) to calculate the relativistic electron beam transport range.

To verify the developed stopping power model given in Eqs. (2) and (3), we calculate the electron transport range with initial energies of 0.5 MeV–20 MeV in DT fuel with gold doping ratio of 0.5%–30% using the stopping power model and Geant4 simulation. The difference δ between the model and Geant4 simulation is shown in Fig. 1. At $\rho = 300$ g/cm^3, the maximum difference is about 6%. At $\rho = 100$ g/cm^3, the difference is basically lower than 10% and the maximum difference of 12%–16% appears in the low electron energy range < 0.5 MeV, which is below the favorable energy range for FI or DCI heating. In the following, our investigation will be based upon the stopping power model and Geant4 simulation.

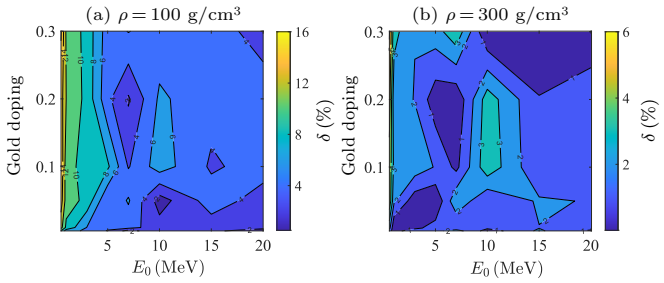


Fig. 1. The difference δ between the stopping power model and Geant4 simulations with the initial fast-electron energies of 0.5 MeV–20 MeV and the gold doping ratio of 0.5%–30%, where the fuel density is taken as $\rho = 100$ g/cm^3 in (a) and $\rho = 300$ g/cm^3 in (b).

Note that we have calculated the difference δ of electron transport ranges between the stopping power model and Geant4 simulation with initial energies of 0.5 MeV–20 MeV in DT fuel with gold doping ratio of 0.5%–30% and density of 180 g/cm^3–700 g/cm^3. The maximum difference δ is basically less than 10%. Therefore, in the typical range of laser fusion we are interested in, the difference between them are not significant.

Furthermore, we examine the influence of the electron beam spread on the transport ranges and the results are shown in Fig. 2. This figure displays the deviations of the average transport ranges between the electron beams with energy spreads and the monoenergetic beam, where the central energies of 1 MeV and 5 MeV are taken. One can see that even with FWHM energy spread of $\Delta E_{\rm FWHM}/E_0 = 50\%$, the difference between the two cases is only 1.27% and 1.02%, respectively.

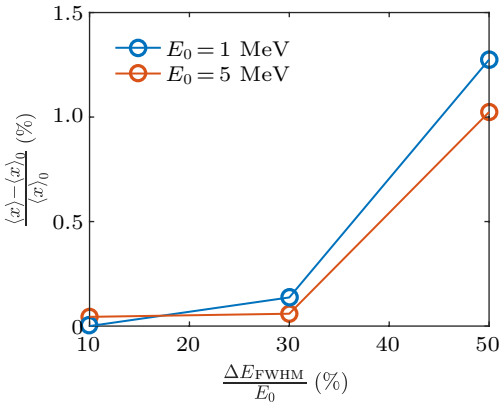


Fig. 2. The deviations between the average electron transport ranges and those of monoenergetic beams as a function of the full-width at half maxima energy spreads, where the central energy is taken as 1 MeV (blue) and 5 MeV (red). In the Geant4 simulation, the plasma density is taken as 300 g/cm^3 and a gold doping ratio is taken as 5%.

3. Effect of gold doping on the electron transport range

We investigate the contribution of the Coulomb collision and bremsstrahlung to the electron transport in gold doped fuel. We find that with the growth of the electron energy and gold doping ratio, the contribution proportion of the bremsstrahlung increases and that of the collision decreases. Therefore, the radiative losses of high-energy electrons by bremsstrahlung should be considered seriously.

To quantify the contribution of Coulomb collision and bremsstrahlung due to gold doping, we calculate the electron transport range in three cases using the stopping power model. In case 1, we calculate the electron range $\langle x\rangle_{\rm DT}$ in uniform DT plasma by the collision. In case 2, we calculate the electron range $\langle x\rangle_{\rm Au}$ in gold doped DT plasma by the collision. In case 3, we calculate the electron range $\langle x\rangle_{\rm Au-brem}$ in gold doped DT plasma both by the collision and bremsstrahlung. We use $(\langle x\rangle_{\rm DT} - \langle x\rangle_{\rm Au})/\langle x\rangle_{\rm DT}$ to quantify the contribution of the collisions between electrons and gold ions, which tends to increase the deflection angle and leads to the decrease of the electron range. We use $(\langle x\rangle_{\rm Au} - \langle x\rangle_{\rm Au-brem})/\langle x\rangle_{\rm Au}$ to quantify the contribution of the bremsstrahlung, which also causes the electron range to be reduced.

Figure 3(a) displays $(\langle x\rangle_{\rm DT} - \langle x\rangle_{\rm Au})/\langle x\rangle_{\rm DT}$ representing the contribution of the e–Au collisions. It shows that the gold doping plays an important role in the transport and energy deposition of the electrons with the energies ranging from 0.5 MeV to 20 MeV. Particularly, only 0.5% gold doping brings 40% (with 20 MeV electron energy) to 70% (with 0.5 MeV electron energy) reduction in the electron transport range since the transport scattering cross sections of e–Au collisions are proportional to the square of the $Z_{\rm Au}$. This is much larger than the scattering cross section in the pure DT plasma. As the electron energy grows, the range is less affected by the collisions which are weakly correlated with the scattering cross section and the scattering angle should not be significantly changed.

Figure 3(b) presents $(\langle x\rangle_{\rm Au} - \langle x\rangle_{\rm Au-brem})/\langle x\rangle_{\rm Au}$ to illustrate the contribution of the bremsstrahlung. The rate of bremsstrahlung energy emission per unit volume is

$$P_{\rm br} = 5.35\times10^{-31} n_{\rm e} \sum_i \left(n_i Z_i^2\right) E_{\rm e}^{\frac{1}{2}} \ ({\rm W/cm^3}), \qquad (4)$$

and radiative losses are highly dependent on both the ion charge and the electron energy. The transport range of the 5 MeV electron beam is decreased by 4.3% and 7.8% with the gold doping ratios of 0.5% and 10%, respectively. For the 3 MeV electron beam, the decrease of the range becomes 1.5% and 2.3% with the gold doping ratios of 0.5% and 10%, respectively. For the 1 MeV electron beam, the decrease of the range becomes 0.7% and 1.0%, respectively. Therefore, the bremsstrahlung with slight gold doping should not be ignored when the electron energy is higher or much higher than 1 MeV. Note that the bremsstrahlung energy loss rate $({\rm d}E/{\rm d}s)_{\rm rad} = n_{\rm i}\left(\alpha r_0^2\right)\left(E + mc^2\right) Z^2 \Phi_{\rm rad}^{\rm total}$ linearly increases with the electron energy, which results in the decrease of the electron transport range with the growing electron energy.

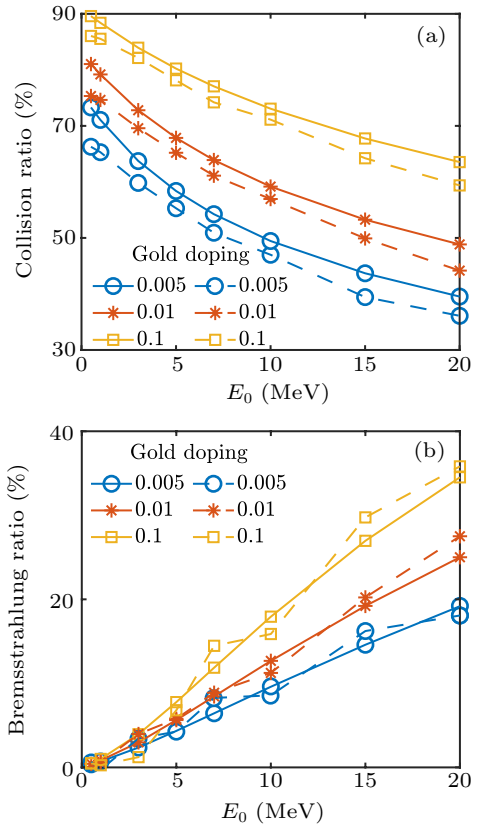


Fig. 3. (a) $\frac{\langle x\rangle_{\rm DT}-\langle x\rangle_{\rm Au}}{\langle x\rangle_{\rm DT}}$ and (b) $\frac{\langle x\rangle_{\rm Au}-\langle x\rangle_{\rm Au-brem}}{\langle x\rangle_{\rm Au}}$ versus the initial electron energy, where the lines with different colors correspond to different gold doping ratios of 0.5% (blue), 1% (red), and 10% (yellow) and the solid and dashed lines are obtained according to the stopping power model and the Geant4 simulations. The plasma density is taken as 300 g/cm^3.

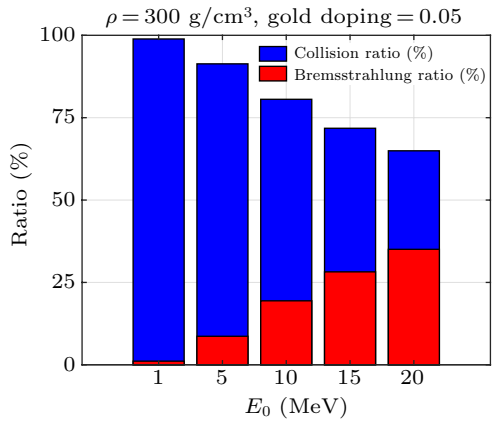


Fig. 4. The electron transport ranges are affected by the e–Au collisions ratio (blue) and bremsstrahlung ratio (red) at different initial electron energy E_0 according to the stopping power model, where we take the plasma density of 300 g/cm^3 and the gold doping ratio of 5% (The collision ratio and radiation ratio are normalized in such a way that $\frac{\langle x\rangle_{\rm DT}-\langle x\rangle_{\rm Au}}{\langle x\rangle_{\rm DT}}+\frac{\langle x\rangle_{\rm Au}-\langle x\rangle_{\rm Au-brem}}{\langle x\rangle_{\rm Au}}=1$).

One can also observe in Fig. 3 that the influence of the bremsstrahlung and the e–Au collision on the electron range reduction appears to exhibit opposite trends with the increase of the electron energy. With lower electron energies, the e–Au collision dominates over the bremsstrahlung effect. With higher electron energies, the e–Au collision tends to have the similar level of contributions to the bremsstrahlung effect. The two effects result in the gold doping even at a low level of 0.5% being important in the relativistic electron transport in high density fuel in DCI or FI. The comparison between the e–Au collisions and bremsstrahlung is shown more clearly in Fig. 4, where the plasma density is taken as 300 g/cm^3 and the gold doping ratio is taken as 5%. One can see that the decrease of the electron transport range with the electron beam of 1 MeV is almost entirely caused by e–Au collisions. For the electron beam of 20 MeV, the bremsstrahlung cannot be ignored, and it contributes more than half of the collisions.

It should be pointed out that the Geant4 simulations give similar results and the same trend as the stopping power model. In the Geant4 code, the fuel is considered to be a cold target but not a plasma state, so the probability of large angle scattering of electrons above 50 keV is overestimated to some degree, resulting in the electron range somewhat less than that obtained by the stopping power model.

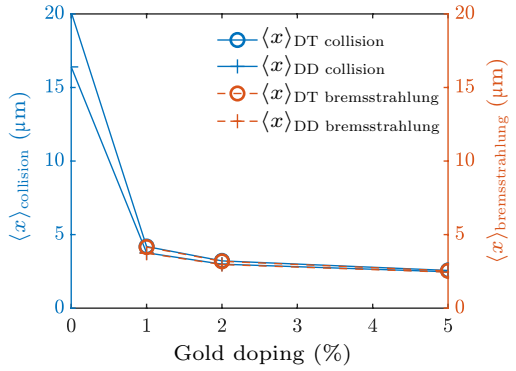


Fig. 5. The electrons transport ranges $\langle x\rangle$ affected by the collision (left axis) and bremsstrahlung (right axis) versus the gold doping ratio in DD and DT targets, respectively. In the calculations, the initial electron energy is taken as 1 MeV and the plasma density is taken as 300 g/cm^3.

We have also performed calculations with DD targets. The electron transport ranges in DD targets differ from those in DT targets due to the modified mass number A of the background plasma ($A = 2.5 \rightarrow A = 2$). This reduced ion mass number A leads to an increased ion number density $n_{\rm i} = N_{\rm A}\rho/A$ and larger transport cross sections for ion scattering. Consequently, the enhanced collisions between the electron and DD ions result in a significant reduction in the electron beam range, as shown in Fig. 5. This figure presents the ranges of 1 MeV electrons in DD and DT targets with different gold doping ratios. As the gold doping ratio in the fuel increases, the deviations in electron range between DD and DT targets become progressively smaller. The reason is that the doping of high Z gold makes the transport scattering cross sections less sensitive to changes in the mass number A. A comparison between the electron transport ranges affected by collisions and those affected by bremsstrahlung shows that the mass number has little effect on the electron range via bremsstrahlung. This indicates that the substitution of DT targets with DD targets primarily influences the electron transport ranges through collision rather than bremsstrahlung.

4. Influence of spherical target on electron beam transmission

In the last section, we have investigated electron transport in an infinite target, which is a conventional configuration and frequently discussed in the literature. In this case, the transverse broadening of the electrons in transport is not considered in the energy coupling efficiency to the target[46–48] as well as all of the bremsstrahlung photons that are reabsorbed since the target is infinite. Here, we discuss the electron transport in a spherical target with a typical areal density. In this configuration, the effects of electron transverse broadening and escape of the bremsstrahlung photons away from the finite target can be appropriately considered.

We use Geant4 to simulate an electron beam transport in a spherical target with an areal density of $\rho R = 1$ g/cm^2 with different gold doping ratios. As the doping ratio increases, the number of electrons around the axis decays more rapidly, which hinders the target heating. With the growth of the electron beam energy, the total energy of the bremsstrahlung photons increases, but the total energy of the photons reabsorbed by the target decreases.

Figure 6 shows the electron number distribution as a function of the transverse position (x) at two longitudinal positions ($z = 3$ μm and 7 μm). One can observe that the transverse broadening of electron beam transport in dense fuels with different gold doping ratios, which also shows the influence of gold ratios on the transverse broadening. Comparison of 2% and 5% gold doping can illustrate that higher gold doping ratio results in stronger transverse broadening of the electron beam because electrons collide more frequently with gold ions, leading to large-angle scattering. Consequently, higher gold doping impairs the electron transport and target heating. One can also see that with the growth of the electron energy the transverse broadening is weaker. At a smaller longitudinal position $z = 3$ μm, the electrons roughly follow a normal distribution in the transverse direction. As the electrons transport deeper into the target and collide with the target, the electrons tend to gradually deflect outward, and only a minority of electrons can maintain on a straight trajectory.

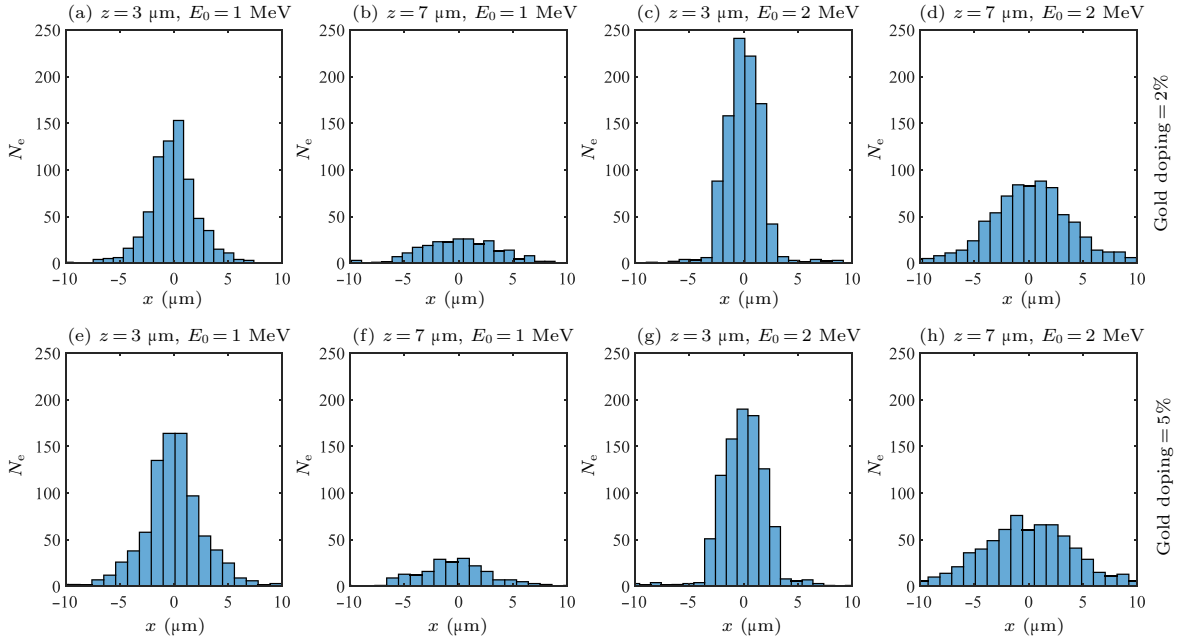


Fig. 6. Electron number distributions at different transverse positions, which are collected in the longitudinal positions $z = 3$ μm [(a), (c), (e), (g)] and 7 μm [(b), (d), (f), (h)]. In the Geant4 simulations, we calculate the transport of the electron beam of 1 MeV [(a),(b),(e),(f)] and 2 MeV [(c), (d), (g), (h)] in a DT plasma with 2% [(a)–(d)] and 5% [(e)–(h)] gold doping. The typical areal density of the spherical target is 1 g/cm^2 and the plasma density is 300 g/cm^3.

The influence of the electron beam energy absorbed by the finite spherical target can be more clearly observed in Fig. 7. The increases of initial electron energy and gold doping ratio cause the decrease of the electron energy absorption. For 2% gold doping ratio, the electron energy absorption proportion is 71% with the initial energy of 1 MeV and it significantly decreases to 17.7% with the initial energy of 10 MeV. This is due to the fact that the range of the higher-energy electron beams is much greater than the target size. With the given initial energy of 2 MeV, the energy absorption proportion is 75.8% with the gold doping ratios of 0.5% and it decreased to 58.1% with the gold doping ratios of 10%, where the bremsstrahlung radiation loss has been counted. The energy absorption is lowered with the growing gold doping ratio because the doped gold leads to the increase in electron energy loss due to bremsstrahlung.

In contrast to the infinite target which can absorb all the bremsstrahlung photons, the finite target significantly influences the reabsorption of the bremsstrahlung photons. Figure 8 displays spectra of the generated bremsstrahlung photons and the photons reabsorbed by the target. Figures 8(a)–8(c) illustrate the energy of the reabsorbed photons is mainly dis-

tributed below 200 keV, since relatively soft x-rays are more easily reabsorbed by the target. For the electron beams of 1 MeV and 5 MeV, the total generated photon energy accounts for 2.59% and 10.3% of the electron energy and the reabsorbed photons energy accounts for 31.6% and 8.93% of the total bremsstrahlung photons energy, respectively. Basically, as the electron initial energy increases, the electrons lose more energy via the bremsstrahlung, but the photon reabsorption decreases. In Figs. 8(d)–8(f), we proceed to simulate electron beams of 1 MeV transported in the spherical target with gold doping ratios of 0.5%, 2%, and 5%, respectively. As the gold ratio increases, the total energy of both the generated photons and the reabsorbed ones grows.

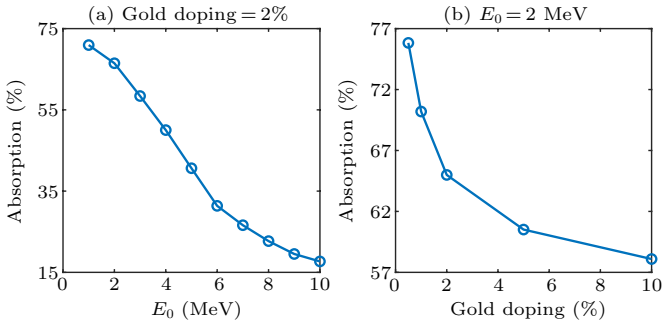


Fig. 7. The proportion of the electron energy absorbed by the spherical target as a function of the initial electron energy (a) and the gold doping ratio (b), where the gold doping ratio is taken as 2% in (a) and the initial electron energy is taken as 2 MeV in (b). In the Geant4 simulation, the target is taken with an areal density of $\rho R = 1$ g/cm^2 and a density of 300 g/cm^3.

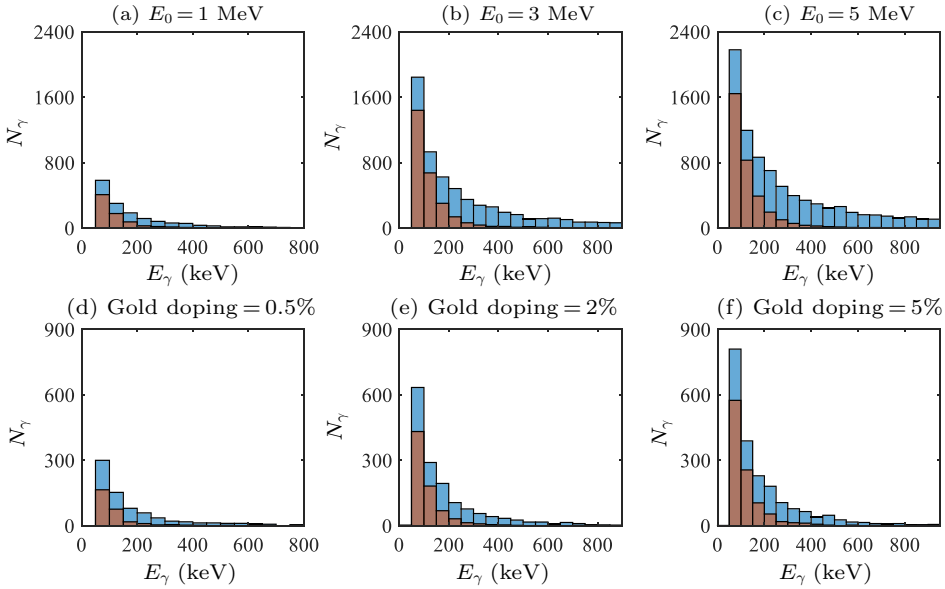


Fig. 8. Spectra of the generated bremsstrahlung photons (blue bars) and the photons reabsorbed by the target (brown bars), obtained from the Geant4 simulations. The gold doping ratio of 2% is fixed in the first row and different initial electron energies of $E_0 = 1$ MeV, 3 MeV, and 5 MeV are taken in (a)–(c), respectively. The initial electron energy $E_0 = 1$ MeV is fixed in the second row and different gold doping ratios of 0.5%, 2%, and 5% are taken in (d)–(f), respectively. The target is taken with an areal density of $\rho R = 1$ g/cm^2 and a density of 300 g/cm^3.

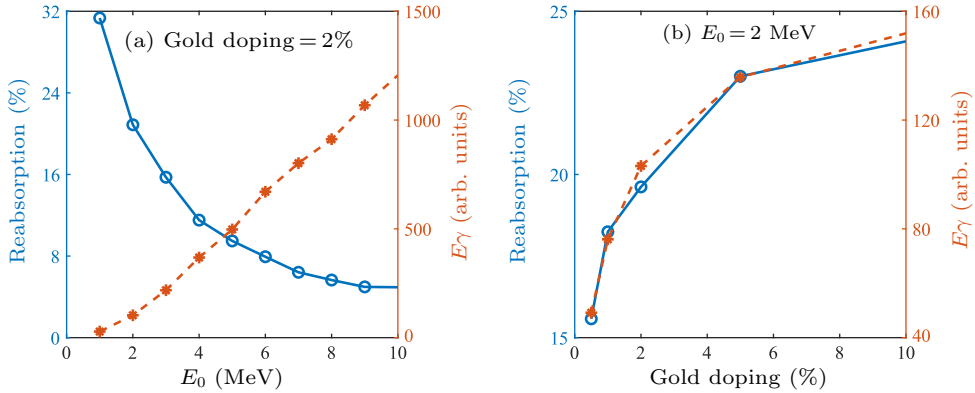


Fig. 9. The proportion of the bremsstrahlung photon energy (blue solid line with circles) reabsorbed by the target and the total energy of bremsstrahlung photons (orange dashed line with stars) versus the electron initial energy in (a) and the gold doping ratio in (b). The gold doping ratio is taken as 2% in (a) and the electron energy is taken as 2 MeV in (b). The spherical target is taken with the areal density 1 g/cm^2 and the density 300 g/cm^3.

Figure 9 presents the generated bremsstrahlung photons and the photons reabsorbed versus the electron initial energy and the gold doping ratio. It is more clearly shown that as the electron initial energy increases, the total photon energy increases approximately linearly and the reabsorbed photon energy dramatically decreases from 31.3% (with 1 MeV elec-

tron energy) to 4.94% (with 10 MeV electron energy). The increased energy of the escaped photons is harmful to fuel heating. The photons are more likely to be captured when the target has a higher gold doping ratio, as presented in Fig. 9(b). The photon reabsorption increases from 15.6% (with 0.5% gold doping ratio) to 24.1% (with 10% gold doping ratio).

5. Conclusion

In the context of DCI scheme and FI, based on the range of electron transport in pure DT fuel, this paper develops a stopping power model that takes into account gold doping and modifies the calculations for collision and bremsstrahlung in gold doping DT fuels. Using the developed stopping power, we investigate the transport range of electrons with different gold doping ratios. We find that as the initial energy of the relativistic electron beam increases, the contribution of Coulomb collision to the electron range gradually decreases, while bremsstrahlung linearly increases significantly. For example, when the initial energy of the electron beam is raised from 1 MeV to 5 MeV and transported into a plasma with 5% gold doping, bremsstrahlung causes the electron range to drop from 0.98% to 17.1%. Then, Geant4 simulates the transport of relativistic electron beams in a finite spherical fuel. We observe that increasing the gold doping ratio in the fuel leads to more rapid decay of electrons around the axis and negatively affects the proportion of electron energy absorbed by the target. Furthermore, the partial bremsstrahlung photon energy loss may be reabsorbed by the finite fuel. Geant4 simulation indicates that as the initial energy of electrons increases from 1 MeV to 5 MeV in a spherical target doped with 2% gold, the fraction of energy in generated photons relative to the total electron beam energy increases from 2.59% to 10.3%. However, the probability of photon energy being reabsorbed decreased from 29.9% to 9.24%, significantly reducing the efficiency of electron energy utilization. Finally, the initial energy of the electron beam ranges from 1 MeV to 10 MeV, the proportion of photon absorption declines from 31.3% to 4.94%, which significantly lessens the electron energy deposition.

Appendix A: Comparison between the stopping power model and Geant4 simulation

We calculate the range of the relativistic electron beam with the initial energy ranging from 0.3 MeV to 10 MeV (with an energy interval of 0.01 keV) in uniform pure DT fuel with the density of 50 g/cm^3–300 g/cm^3. Figure A1 show that there is little difference among the stopping power, Betti's empirical formula, and Geant4 simulation.

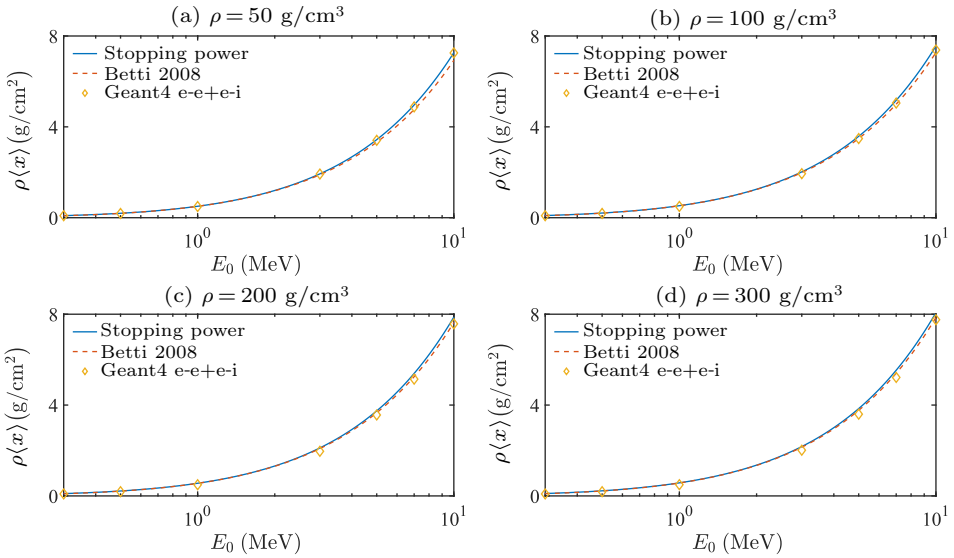


Fig. A1. Electron range areal density $\rho\langle x\rangle$ of 0.3 MeV–10 MeV with the plasma density of $\rho = 50$ g/cm^3 in (a), $\rho = 100$ g/cm^3 in (b), $\rho = 200$ g/cm^3 in (c) and $\rho = 300$ g/cm^3 in (d), where in each plot the blue solid line corresponds to the stopping power, the red dotted line to the Betti's empirical formula, and the yellow diamond line to the Geant4 simulation, respectively.

Acknowledgements

Project supported by the Strategic Priority Research Program of Chinese Academy of Sciences (Grant Nos. XDA25050300 and XDA25010100), the National Key R&D Program of China (Grant No. 2018YFA0404801), the Fundamental Research Funds for the Central Universities, and the Research Funds of Renmin University of China (Grant No. 20XNLG01). Computational resources have been provided by the Physical Laboratory of High Performance Computing at Renmin University of China.

References

[1] Nuckolls J, Wood L, Thiessen A and Zimmerman G 1972 *Nature* **239** 139
[2] Lindl J D, McCrory R L and Campbell E M 1992 *Phys. Today* **45** 32
[3] Lan K, Dong Y S, Wu J F, Li Z C, Chen Y H, Cao H, Hao L, Li S and Ren G L 2021 *Phys. Rev. Lett.* **127** 245001

[4] Li X, Dong Y S, Kang D G, Jiang W, Shen H, Kuang L Y, Zhang H S, Yang J M and Wang Q 2022 *Phys. Rev. Lett.* **128** 195001
[5] Zhang F, Cai H B, Zhou W M, *et al.* 2020 *Nat. Phys.* **16** 810
[6] Lan K 2022 *Matter Radiat. Extremes* **7** 055701
[7] Sui Z and Lan K 2024 *Matter Radiat. Extremes* **9** 043002
[8] Skupsky S and Lee K 1983 *J. Appl. Phys.* **54** 3662
[9] Taylor R J, Velikovich A L, Dahlburg J P and Gardner J H 1997 *Phys. Rev. Lett.* **79** 1861
[10] Cole A J, Kilkenny J D, Rumsby P T, Evans R G, Hooker C J and Key M H 1982 *Nature* **299** 329
[11] Hurricane O A, Callahan D A, Casey D T, Celliers P M, Cerjan C, Dewald E L, Dittrich T R, Döppner T, Hinkel D E, Berzak Hopkins L F, Kline J L, Le Pape S, Ma T, MacPhee A G, Milovich J L, Pak A, Park H S, Patel P K, Remington B A, Salmonson J D, Springer P T and Tommasini R 2014 *Nature* **506** 343
[12] Le Pape S, Berzak Hopkins L F, Divol L, *et al*. 2018 *Phys. Rev. Lett.* **120** 245003
[13] Baker K L, Thomas C A, Casey D T, *et al*. 2018 *Phys. Rev. Lett.* **121** 135001
[14] Abu-Shawareb H, Acree R, Adams P, *et al*. 2022 *Phys. Rev. Lett.* **129** 075001
[15] Abu-Shawareb H, Acree R, Adams P, *et al*. 2024 *Phys. Rev. Lett.* **132** 065102
[16] Hurricane O A, Callahan D A, Casey D T, Christopherson A R, Kritcher A L, Landen O L, Maclaren S A, Nora R, Patel P K, Ralph J, Schlossberg D, Springer P T, Young C V and Zylstra A B 2024 *Phys. Rev. Lett.* **132** 065103
[17] Rubery M S, Rosen M D, Aybar N, *et al*. 2024 *Phys. Rev. Lett.* **132** 065104
[18] Tabak M, Hammer J, Glinsky M E, Kruer W L, Wilks S C, Woodworth J, Campbell E M, Perry M D and Mason R J 1994 *Phys. Plasmas* **1** 1626
[19] Murakami M and Nagatomo H 2005 *Nucl. Instrum. Methods Phys. Res. Sect. A* **544** 67
[20] Murakami M, Nagatomo H, Azechi H, Ogando F, Perlado M and Eliezer S 2006 *Nucl. Fusion* **46** 99
[21] Azechi H, Sakaiya T, Watari T, *et al*. 2009 *Phys. Rev. Lett.* **102** 235002
[22] Betti R, Zhou C D, Anderson K S, Perkins L J, Theobald W, and Solodov A A 2007 *Phys. Rev. Lett.* **98** 155001
[23] Nora R, Theobald W, Betti R, *et al*. 2015 *Phys. Rev. Lett.* **114** 045001
[24] Velarde P, Ogando F, Eliezer S, Eliezer S, Martinez-val J M, Perlado J M and Murakami M 2005 *Laser Part. Beams* **23** 43
[25] Zhang J, Wang W M, Yang X H, Wu D, Ma Y Y, Jiao J L, Zhang J, Wu F Y, Yuan X H, Li Y T and Zhu J Q 2020 *Phil. Trans. R. Soc. A* **378** 20200015
[26] Wang W M, Gibbon P, Sheng Z M and Li Y T 2015 *Phys. Rev. Lett.* **114** 015001
[27] Zhou G, Wang W M, Li Y T and Zhang J 2022 *Phys. Plasmas* **29** 052704
[28] Zhang T H, Wang W M, Li Y T and Zhang J 2022 *Phys. Rev. E* **106** 055211
[29] Liu Z D, Zhong J Y, Yuan X H, *et al*. 2023 *Chin. Phys. B* **32** 110702
[30] Zhu Z Y, Liu Y X, Li Y J and Zhang J 2022 *Chin. Phys. B* **31** 105202
[31] Zhang C L, Zhang Y H, Yuan X H, *et al*. 2024 *Chin. Phys. B* **33** 025201
[32] Zhu Z Y, Zhang C L, Li Y J and Zhang J 2024 *Chin. Phys. B* **33** 065203
[33] Xie Y K, Zhang C L, Cheng Y Z and Li Y J 2024 *Chin. Phys. B* **33** 125203
[34] Chen Z Y, Zhao K G and Li Y J 2024 *Chin. Phys. B* **33** 115202
[35] Kodama R, Norreys P, Mima K, *et al*. 2001 *Nature* **412** 798
[36] Agostinelli S, Allison J, Amako KA, *et al*. 2003 *Nucl. Instrum. Methods Phys. Res. A* **506** 250
[37] Deutsch C, Furukawa H, Mima K, Murakami M and Nishihara K 1996 *Phys. Rev. Lett.* **77** 2483
[38] Li C K and Petrasso R D 2004 *Phys. Rev. E* **70** 067401
[39] Li C K and Petrasso R D 2006 *Phys. Rev. E* **73** 016402
[40] Li C K and Petrasso R D 2006 *Phys. Plasmas* **13** 056314
[41] Solodov A A and Betti R 2008 *Phys. Plasmas* **15** 042707
[42] Atzeni S, Schiavi A and Davies J R 2009 *Plasma Phys. Control. Fusion* **51** 015016
[43] Lewis H W 1950 *Phys. Rev.* **78** 526
[44] Seltzer S M and Berger M J 1985 *Nucl. Instrum. Methods Phys. Res. B* **12** 95
[45] Seltzer S M and Berger M J 1986 *At Data Nucl Data Tables* **35** 345
[46] Strozzi D J, Tabak M, Larson D J, Divol L, Kemp A J, Bellei C, Marinak M M and Key M H 2012 *Phys. Plasmas* **19** 072711
[47] Stephens R B, Snavely R A, Aglitskiy Y, *et al*. 2004 *Phys. Rev. E* **69** 066414
[48] Sheng Z M, Sentoku Y, Mima K, Zhang J, Yu W and Meyer-ter-Vehn J 2000 *Phys. Rev. Lett.* **85** 5340